Collisional detachment in collisions of Cl^- with the rare gases

R. L. Champion and L. D. Doverspike
Department of Physics, College of William and Mary, Williamsburg, Virginia 23185
(Received 10 July 1975)

Absolute total electron detachment and relative elastic differential cross sections for the scattering of Cl^- by Ne, Ar, Kr, and Xe have been measured at energies ranging from near detachment threshold to 180 eV. The experimental results have been analyzed by using semiclassical expressions for the cross sections which involve localized complex potentials. Reasonable potentials have been deduced which yield calculated cross sections that are in good agreement with the experimental observations.

I. INTRODUCTION

Previous work in this laboratory has concentrated on the quantitative understanding of the collisional detachment of electrons from negative atomic ions.[1] In these studies a local complex-potential model was used to analyze relative differential elastic-scattering experiments which were related to the low-energy collisional detachment of electrons from H^- and D^- by helium.

In the complex-potential model, electron detachment is attributed to the crossing of the negative-ion bound state with the continuum of states representing a neutral molecule and free electron. We have restricted our investigations to those systems for which the neutral molecular state is unbound: Consequently, associative detachment is prohibited. Within the framework of this model (given the complex potential for a negative ion-atom system) one can derive expressions for (i) the total cross section for electron detachment, (ii) the differential cross section for elastic scattering of the negative ions, (iii) the differential cross section for the "fast" neutrals formed in the detachment process, and (iv) the kinetic-energy distribution of the detached electrons. Also the model predicts the existence of an isotope effect which was confirmed in measurements of the differential elastic cross sections for the H^- (D^-) + He systems.[1]

For systems in which only detachment and elastic scattering are important, the onset of electron detachment can manifest itself as an abrupt decrease in the differential elastic cross section beyond some scattering (threshold) angle: This effect arises because of the depletion of the elastic channel by the detachment process. The threshold angle corresponding to the onset of detachment can be related to the crossing point of the molecular states involved in the collision. No distinct threshold was observed in the H^- (D^-) + He experiments: Only a downward curvature in the differential elastic cross sections (over a rather broad range of scattering angles) could be discerned. However, it was established that these results could be made compatible with the complex-potential theory at low collision energies, but some deviations appeared at higher energies.

In a continuing effort to provide critical experimental tests of the local complex-potential theory of collisional detachment, we present here the results and analyses of a series of scattering experiments involving Cl^- and the rare gases Ne, Ar, Kr, and Xe. For each combination the absolute total-electron-detachment cross section has been measured over the energy range from threshold to approximately 180 eV, and also the relative elastic differential cross section has been measured at various energies within this range. The results are analyzed within the complex-potential framework.

These particular systems were investigated for several reasons: First, they are systems for which the real parts of the ionic potentials are available (over a rather limited range of internuclear distances). The potentials were determined by Boerboom *et al.*[2] in experiments which were sensitive to the ionic potentials over a small range of internuclear separations outside the crossing points of the ionic and neutral states, i.e., to regions of the potentials in which electron detachment is prohibited. In addition to the above potentials, model calculations are also available.[3] Furthermore, favorable mass ratios and the large electron affinity of chlorine (3.6 eV) make the detachment-threshold regions more accessible to experimental investigation. Finally, in these systems the collision velocities are small compared to those for the H^- (D^-) systems (at the same relative energy). Consequently, the detachment thresholds should be much more pronounced in the elastic differential cross sections, thereby making it rather easy to accurately determine where the molecular states cross one another.

Descriptions of the apparatus and experimental procedures utilized in the present studies are

presented in Sec. II. Section III contains a brief explanation of the theory employed in the analysis of the data. The data are then presented and analyzed in Sec. IV.

II. EXPERIMENTAL APPARATUS AND PROCEDURE

A. Differential cross-section measurements

Measurements of the relative elastic-scattering differential cross sections for Cl^- on the rare gases are performed on an apparatus which has been described in detail previously.[4] The negative-ion beam is produced in a duoplasmatron ion source (which uses a 4:1 mixture of Argon and CCl_4 as the source gas) and subjected to mass analysis. The collision chamber contains the target gas at low pressure (~0.5 mTorr) and the scattered Cl^- ions are transmitted through a 127° cylindrical electrostatic-energy analyzer followed by a quadrupole radiofrequency mass spectrometer. Typical angular and energy spreads of the primary ion beam are 1.5° and $0.03E_1$, respectively, where E_1 is the laboratory collision energy. Both figures represent the full widths at half-maximum.

B. Total-electron-detachment cross-section measurements

Measurements of the absolute total-electron-detachment cross sections are performed on an apparatus which used a duoplasmatron ion source identical to that just mentioned. The Cl^- ions are energy selected with a 90° parallel-plate electrostatic selector and are subjected to momentum analysis by a Wien filter.

1. Scattering region

After passing through the Wien filter, the primary ions are focused into the scattering region which is shown schematically in Fig. 1. This region contains a cylindrical collision chamber B, followed by three parallel (~95% transparent) tungsten grids, *I–III*, and a Faraday collector C. The collision chamber is wrapped with magnet wire to provide an axial magnetic field in the chamber. An electron trap for detached electrons is produced in the region between plate A and grid *II*, when a slightly negative bias is applied to grid *II* and the magnetic field is turned on. With this arrangement, low-energy detached electrons are repelled by grid *II* and are necessarily collected on element A due to their rather small cyclotron radius. It was necessary to go to this collection technique rather than use the conventional method of collecting the detached electrons on the elements A and B, because large-angle elastic scattering of Cl^- dominated the signal on element B at low collision energies.

A thin guard ring extends into the scattering chamber slightly beyond the surface of element A to prevent Cl^- ions (which may collide with the inner wall of the aperture) from reaching element A. The scattering-path length is defined as that distance (4.643 cm) between the end of the guard ring and grid *II*. The primary-beam current is measured at the Faraday cup C, which is biased positively with respect to grid *III* to suppress secondarily emitted electrons. The guard ring, elements A and B, and grid *I* are operated at ground potential, and grid *III* and the Faraday cup are at positive potentials to prevent detached electrons formed in the region past grid *II* from reaching element A. Grid *II* is biased several volts negative to form the electron trap, and it was found that the electron current collected on A does not depend upon the voltage on grid *II* over the range $-5 \leq V \leq -1$ V.

With the elements of the scattering chamber biased as indicated above, the current collected on element A, I_A, can be monitored as a function of the applied axial magnetic field $\vec{B}$. As $\vec{B}$ is increased, the cyclotron radii of the detached electrons decrease and I_A increases until the point is reached where $(mcV_{max})/qB < R_A$, where V_{max} is the maximum transverse component of the detached electron's velocity vector and R_A is the radius of element A. As $\vec{B}$ is increased further (beyond about 5 G), I_A may decrease slightly owing to electrons being channeled back through the small entrance aperture of the scattering chamber.

As might be expected, some electrons will be collected on element A even when no target gas is in the scattering chamber (i.e., the pressure is ~5×10^{-8} Torr). This is primarily due to detached electrons resulting from collisions of the ion

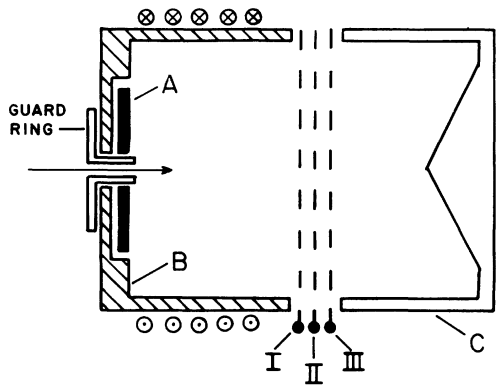

FIG. 1. Schematic diagram of the collision region.

beam with grids *I* and *II*. The effect of these "gas-out" electrons is small and can be subtracted from the "gas-in" reading to give an accurate indication of the intensity of the electrons detached by gas phase conditions.

A plot of I_A vs $\vec{B}$ is given in Fig. 2 for both the gas-in and gas-out conditions and is representative of such curves obtained at all collision energies. As can be seen in Fig. 2 the difference, I_A (gas in) $- I_A$ (gas out), maximizes in the neighborhood of ~5 G, and such a maximum is used to compute the total-detachment cross section.

The laboratory energy of the primary ion beam can be determined by retarding with grid *II* and monitoring the current to element *C*. The derivative of the $I_C(V)$ curve yields a curve of approximately Gaussian shape whose centroid is taken to be the beam energy. For all the total-cross-section experiments reported here, the laboratory energy spread of the primary beam is ~5 eV, full width at half-maximum.

2. *Pressure measurements*

The pressure of the target gas in the scattering chamber is measured by an MKS Baratron capacitance manometer. The device has been calibrated by means of an absolute oil manometer operated by the Flight Instrumentation Division of NASA-Langley for such purposes. The Baratron was found to be accurate to within 4% of the manufacturers stated calibration (it read low) and the calibration was reproducible to within 0.5% for three different calibrations. The scattering chamber was at a temperature of 300 °K while the Baratron head was maintained at 322 °K, thus necessitating a slight correction due to thermal transpiration when the target-gas number density is computed.

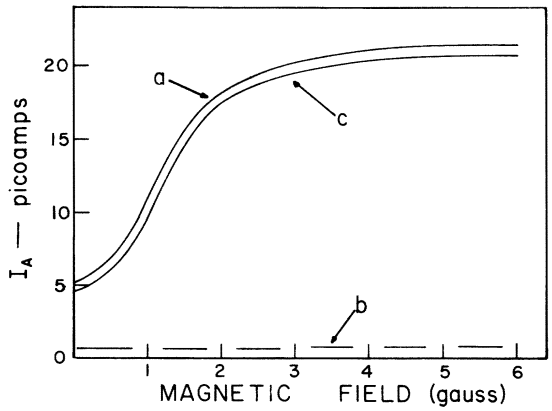

FIG. 2. Current collected on element *A* as a function of applied magnetic field with scattering gas in (a) and out (b). The difference is represented by (c) and the experiment is Cl^- + Kr at $E \simeq 23$ eV.

All target-gas pressures were maintained between 0.3 and 0.4 mTorr in the present experiments. A study of the dependence on pressure of the function

$$\ln(1 - I_{SCAT}/I_0)$$

was performed over the target-gas pressure range 0.0–2 mTorr and was found to be extremely linear in this pressure interval.

3. *Corrections due to the grids*

The effect of grids *I–III* is to absorb a fraction of both the primary ion beam and the detached electrons. In the former case, the current reaching the Faraday cup *C* is less than that in the scattering chamber owing to absorption by the three grids. By turning the primary beam around with grid *I* and measuring the ion current collected on elements *A* and *B*, it was determined that the grids attenuated $(14 \pm 1)\%$ of the primary beam. This number was confirmed by measuring the current to each of the grids independently when the primary beam was allowed to pass through all three grids. The attenuation was found to be independent of the primary-beam energy and is very close to what would be predicted by the optical transparency of the grids.

Some (~50%) of the detached electrons must pass through grid *I* twice before being collected on element *A*, causing some absorption of the detached electrons, namely $(2 \pm 2)\%$.

Including the above corrections, the cross section is then determined by

$$\sigma = -[\ln(1 - 1.02 I_A/1.14 I_C)]/nl$$

where l is the path length mentioned previously and n is the number density given by

$$n = \frac{9.658 \times 10^{15}}{(300 \times 322)^{1/2}} P \text{ cm}^{-3}$$

where P is expressed in 10^{-3} Torr and the denominator is the geometric average of the scattering-cell temperature and that of the capacitance manometer head and accounts for the effect of thermal transpiration. Experimental results determined by the above procedure are thought to be accurate to $\mp 10\%$ and reproducible to within $\pm 6\%$.

III. THEORY

Only a brief outline of the complex-potential model will be given since a complete discussion of the model is presented in Ref. 1. At infinite separation the potential curves for the $X + Cl^-$ systems (where X = Ne, Ar, Kr, Xe) lie 3.6 eV below the corresponding neutral curves of $X + Cl$. Since the detached electron can have any positive

energy, the total electronic energy of the (X + Cl + free e^-) system must be regarded as a continuum of parallel curves.

For distances less than some R_x, the energy of the negative molecular ion (XCl^-) lies above the energy of the neutral molecule (XCl). In this region the electron can no longer be regarded as bound, and therefore, the negative molecular ion may undergo electron detachment. Thus the energy of the negative-ion state may be taken as complex, $W(R) = V(R) - \frac{1}{2}i\Gamma(R)$ for $R < R_x$ and the state decays in time as detachment occurs: The lifetime of the state is inversely proportional to the width $\Gamma(R)$.

A rather simple classical model for electron detachment was used in our previous work.[1] Chen and his co-workers[5,6] have developed a complete formalism for electron detachment based upon the JWKB solution to the time-independent wave equation. In their treatment the JWKB complex phase shifts, $\delta_l = \zeta_l + i\eta_l$, are determined for a local complex potential of the form $V(R) - \frac{1}{2}i\Gamma(R)$. ζ_l and η_l are given by rather complicated expressions and each depends upon both $V(R)$ and $\Gamma(R)$. Expressions for ζ_l and η_l are contained in Ref. 6 and will not be repeated here.

The elastic differential cross section is given by

$$\sigma(\theta) = P_s(\theta) b \Big/ \sin\theta \left| \frac{d\Theta_{\mathrm{JWKB}}}{db} \right| , \tag{1}$$

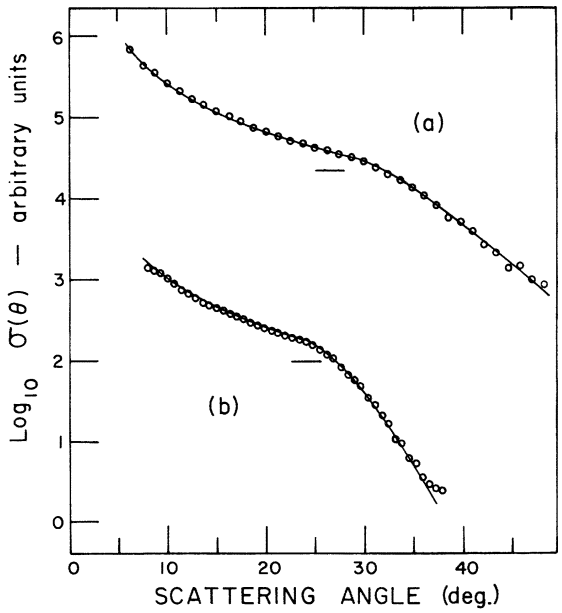

FIG. 3. Differential elastic-scattering cross section (a) Cl^- + Xe at E = 41.7 eV, (b) Cl^- + Kr at E = 47.2 eV. The open circles are the experimental points and the solid lines are results of calculations using parameters of Table I. The horizontal lines adjacent to each curve indicate where the calculated $\sigma_{el}(\theta)$ is $10a_0^2/\mathrm{sr}$.

where $P_s(b) = \exp[-4\eta(b)]$ is the survival probability of the negative ion with respect to electron detachment. In Eq. (1), Θ_{JWKB} is the deflection function which is defined in terms of the real part of the JWKB phase shift, wave number k, and impact parameter, $b = (l + \frac{1}{2})/k$, namely,

$$\Theta_{\mathrm{JWKB}} = \frac{2}{k}\frac{d\zeta(b)}{db} \quad \text{and} \quad \theta = |\Theta_{\mathrm{JWKB}}| .$$

The total-detachment cross section can be written

$$\sigma_{\mathrm{det}} = 2\pi \int_0^{b_x} [1 - P_s(b)] b \, db , \tag{2}$$

where

$$b_x = R_x[1 - V(R_x)/E]^{1/2} ,$$

and E is the c.m. collision energy.

The complex phase shifts as given in Ref. 6 as well as the differential and total cross sections given by Eqs. (1) and (2) are evaluated by appropriate numerical codes and are utilized in the analysis of the experiments reported herein.

IV. EXPERIMENTAL RESULTS

A. Elastic differential cross sections

Relative elastic differential cross sections have been measured for several collision energies for the scattering of Cl^- by the rare gases Ne, Ar, Kr, Xe. Examples of the measured differential cross sections are shown in Figs. 3 and 4. These results show that all the differential cross sections have the same general shape: Each one displays a rather dramatic decrease in magnitude at intermediate scattering angles (due to the depletion of the elastic channel by electron detachment) beginning in the vicinity of $E\theta$ = 1200 eV deg.[7] Otherwise, the differential cross sections are smooth functions of the scattering angle.

B. Absolute total-electron-detachment cross sections

The absolute total-electron-detachment cross sections have been measured for these systems and the results are shown in Figs. 5 and 6. Measurements on Cl^- + (Ne, Ar) extend from threshold to approximately 100 eV, while those for Cl^- + (Kr, Xe) range from 9 to 115 eV. The cross sections all show the same characteristic dependence on collision energy: Each rises rapidly from threshold and becomes almost independent of energy at the highest energies investigated.

C. Analysis

The differential and total cross sections have been calculated with Eqs. (1) and (2). The only

quantities necessary for these calculations are the real and imaginary parts of the ionic potentials. The real parts of the interaction potentials (for all the systems reported here) were initially taken from the work of Boerboom *et al.*[2] They determined incomplete total cross sections for the elastic scattering of Cl^- by He, Ne, Ar, Kr, and Xe in the energy range 2.4–4.0 keV and fit their results with three different potential models. Their best fits were with a screened Coulomb model, $V(R)=(A/R)\exp(-BR)$, and this form has been used in the present calculations. The imaginary portions of the potentials, $\Gamma(R)$, as functions of the internuclear separation R are not known and the following functional form was assumed:

$$\Gamma(R)=\begin{cases}0, & R>R_x\\ F(R_x-R)^{3/2}, & R_1\leq R\leq R_x\\ F(R_x-R_1)^{3/2}, & R<R_1,\end{cases}$$

where R_x is the internuclear separation at which the ionic state crosses the $(XCl+e)$ continuum, and F and R_1 are adjustable parameters. There is some justification of this analytic form if one assumes that the detached electron from Cl^- is a p electron[8] and that the difference in the ionic and neutral (diabatic) potentials is a linear function of R in the vicinity of R_x.

The following procedure was used in all the calculations: (a) The differential elastic cross section $\sigma_{el}(\theta)$ was calculated with Eq. (1) and the corresponding screened Coulomb potential $V(R)$ from Ref. 2. (b) Preliminary estimates of the crossing point R_x and remaining parameters in $\Gamma(R)$ were then determined by comparing the calculated differential cross section with the experimental result. Since the position of the detachment threshold (at fixed collision energy) in $\sigma_{el}(\theta)$ is extremely sensitive to R_x, that parameter is easily deter-

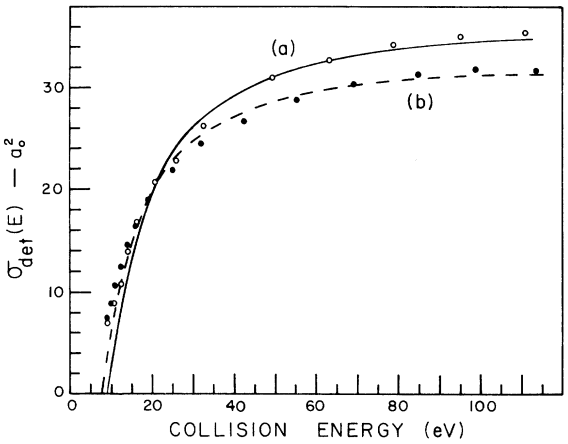

FIG. 5. Absolute total-detachment cross section as a function of collision energy: (a) Cl^-+Xe, (b) Cl^-+Kr. The circles are the experimental points and the dashed and solid lines are the results of calculations using parameters in Table I.

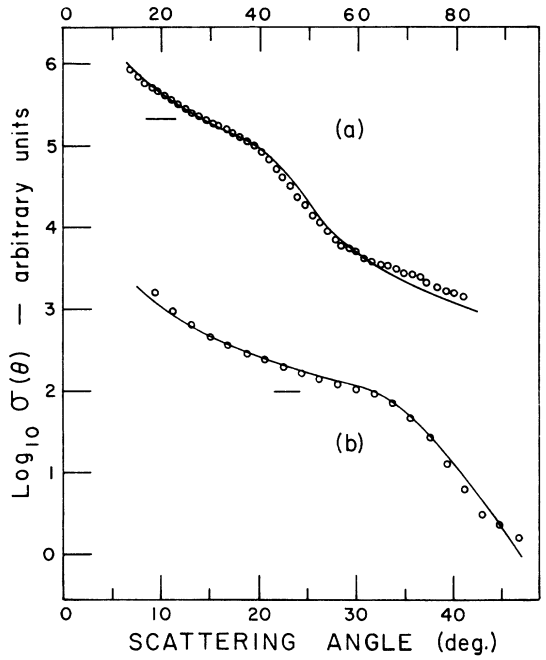

FIG. 4. Differential elastic-scattering cross section (a) Cl^-+Ne at $E=31.9$ eV, (b) Cl^-+Ar at $E=35.7$ eV. The open circles are the experimental points and the solid lines are results of calculations using parameters of Table I. The upper scale refers to curve (a).

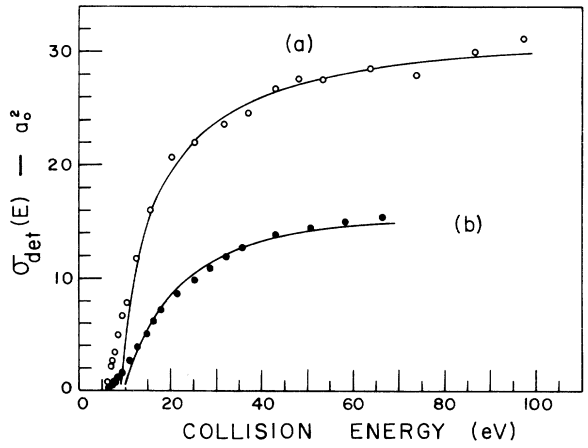

FIG. 6. Absolute total-detachment cross section as a function of collision energy: (a) Cl^-+Ar, (b) Cl^-+Ne. The circles are the experimental points and the solid lines are the results of calculations using parameters in Table I.

mined for given values of A and B in the screened Coulomb potential. The parameter F (and R_1 to lesser extent) determines the shape of $\sigma_{el}(\theta)$ in the detachment region, i.e., for $\theta > \theta_{threshold}$. This procedure allows one to determine R_x to within 0.6% and F to within 10%, given A and B.

The complex potential thus determined is used in conjunction with Eq. (2) to calculate the corresponding total-detachment cross section, $\sigma_{calc}(E)$. However, since only relative differential cross sections are measured, the over-all scale of the complex potential determined in (b) may have to be adjusted in order to fit the measured absolute total cross section, $\sigma_{expt}(E)$. This is accomplished by scaling the parameters in $V(R)$ and $\Gamma(R)$ such that

$$A \to fA, \quad B \to B/f, \quad \text{and} \quad R_x \to fR_x,$$

where the magnitude of f is of the order

$$f^2 \simeq \sigma_{expt}(E)/\sigma_{calc}(E), \quad 40 \lesssim E \lesssim 60 \text{ eV}.$$

It turns out that the fit to $\sigma_{el}(\theta)$, with the newly scaled parameters, remains good as long as $|1-f| \lesssim 7\%$. In the region where the total cross sections are changing rapidly with collision energy (i.e., near threshold), the slopes of the total-detachment cross sections are sensitive to the shape of $V(R)$. Also, in this region the experimental results are affected by spreads in the collision energy caused by thermal motion of the target gas[9] as well as energy spreads in the primary beam. For all these reasons, $\sigma_{calc}(E)$ was adjusted to fit $\sigma_{expt}(E)$ at collision energies between 40 and 60 eV.

The final potentials obtained by the above procedure for the Cl^-–rare-gas systems are listed in Table I. Some specific comments relevant to the individual systems are in order.

1. $Cl^- + (Xe, Kr)$

The measured differential elastic cross sections and the absolute-detachment cross sections are shown in Figs. 3 and 5 for these systems. Calculations of the cross sections using the complex potentials in Table I are shown plotted with the experimental data and good agreement has been obtained between both sets of data and the calculations. The real parts of the potential obtained by fitting the Cl^--Xe,Kr data are in satisfactory agreement with the potentials of Boerboom *et al.*[2]: The parameters A and B differ from those of the latter by only 5.6% for Cl^--Xe and 0.0% for Cl^--Kr. Model calculations of the ionic potential by Gordon and Kim[3] are also in good agreement with $V(R)$ for Cl^--Kr (they did not consider Cl^--Xe).

The magnitude of the potentials for Cl^--Kr and Cl^--Xe at $R = R_x$, i.e., at detachment threshold, are 7.2 eV and 7.6 eV, respectively. Our measurements of the total-detachment sections extend down only to ~9 eV, but any reasonable extrapolation of the measurements to threshold are consistent with the calculated thresholds. In any case, the apparent thresholds will exceed the electron affinity of chlorine by several eV. This demonstrates why such threshold measurements, if used to determine electron affinities, can lead to large errors. A more detailed discussion of the behavior of $\sigma(E)$ near threshold is given in the Appendix.

2. $Cl^- + Ar$

Figures 4 and 6 depict the calculated and experimental results for the differential elastic and total-detachment cross sections. The procedure previously outlined (which used the results of Ref. 2 as the initial estimates of A and B) for determining the potential parameters was incapable of yielding a staisfactory fit to both $\sigma_{el}(\theta)$ and $\sigma_{expt}(E)$: $\sigma_{calc}(E)$ was always too small in the threshold region for any respectable fit to the differential cross section. For this reason, the initial estimate for the ionic potential was taken from the work of Gordon and Kim[3] and the final parameters are given in Table I.

As seen in Fig. 4, the experimental and calculated cross sections do not agree as well as those for the Cl^- + (Xe, Kr) systems. This may indicate that, of all the systems investigated here, the use of a screened Coulomb function is least realistic for describing the Cl^--Ar interaction. This suggestion is supported by the results of Boerboom *et al.*[2] which indicate a relatively small value for the screening coefficient B. Our final potential is in fair agreement with Boerboom *et al.* and Gordon and Kim[3] for $R \gtrsim 3.6a_0$, but at smaller R,

TABLE I. Potential parameters for $Cl^- + X$.

Target	A [a] (eVa_0)	B [a] ($1/a_0$)	R_x (a_0)	F ($eV/a_0^{1.5}$)	R_1 (a_0)
Xe	4530 (4291)	1.36 (1.44)	3.73	2.0	3.25
Kr	3062 (3062)	1.39 (1.39)	3.46	4.6	3.00
Ar	2530 (643)	1.37 (1.06)	3.39	5.4	3.07
Ne	826 (888)	1.39 (1.29)	2.61	4.8	2.40

[a] The values in parentheses are from Ref. 2.

lies well above their results. The steeper rise in our potential was essential in order to fit the measured total-detachment cross section.

3. $Cl^- + Ne$

The experimental results for $Cl^- + Ne$ are shown, along with the final calculations, in Figs. 4 and 6. Because of the favorable mass ratio, the differential measurements for this system cover almost twice the angular range (in c.m. system) of the other systems. The onset of detachment is apparent in the differential cross section at around 40°. However, beyond 60° the cross section flattens out and takes on a shape characteristic of the predetachment region. Within the framework of the complex-potential model, this type of behavior in $\sigma_{el}(\theta)$ would be expected if $\Gamma(R)$ decreased for $R < R_1$ rather than remaining constant as in our calculations. The discrepancy between the experimental results and calculation for $\theta > 60°$ in Fig. 4 is due to this effect. It may be that the other systems behave in a similar fashion at larger scattering angles but such behavior was not capable of being observed in our experiments.

The final parameters (A, B^{-1}) in our potential are approximately 7.5% smaller than those of Boerboom *et al.* The potential of Gordon and Kim also lies well above our potential, and would lead to a total cross section roughly double the magnitude of the one measured for this system.

V. DISCUSSION

By using a semiclassical complex-potential model to calculate both the differential elastic and total-detachment cross sections for $Cl^- + X$, reasonable local complex potentials have been recovered which yield calculated cross sections that are in satisfactory agreement with the experimental observations. Furthermore our results for the real portion of the complex potential are in general agreement with those of previous investigations.

The behavior of the differential and total cross sections is quite insensitive to variations in $V(R)$ for $R < R_x$, due primarily to the fact that the survival probability decreases very rapidly as R becomes less than R_x. Consequently, confidence in the accuracy of the screened Coulomb potential parameters is limited to the region $R > R_x$. Additionally, an upper bound to the range of validity can be established as $R \lesssim 4.5a_0$ due to the lack of small-angle differential-scattering data. Within this range, $R_x \lesssim R \lesssim 4.5a_0$ (and given the limited flexibility of the screened Coulomb potential model), the potential parameters should be accurate to within 10%.

The primary aim of this study was to investigate the usefulness of a local complex potential as an adequate description of the discrete-continuum interaction associated with negative ion-atom collisions. For the energy range of this investigation, the use of a local complex potential along with semiclassical expressions for the cross sections appear to offer a quite appropriate description of the collision dynamics for negative ion-atom collisions. Furthermore the maximum width of the resonance $[\Gamma(R)]$ retrieved from the data is not large (~1 eV for all reactants), which should be necessary if the complex-potential model is to be applicable. The motivation for using the particular analytic form for $\Gamma(R)$ $[\Gamma(R) \sim (R_x - R)^{3/2}]$ has been discussed, and it should be mentioned that this choice tends to give $\sigma_{calc}(E)$ which is in better agreement with $\sigma_{expt}(E)$ than a similar calculation of $\sigma(E)$ which uses a linear or square root dependence on $(R_x - R)$ for $\Gamma(R)$. Specifically, these latter choices for $\Gamma(R)$ tend to give too large a value for $\sigma(E)$ in the intermediate energy range of the experiments (20–30 eV). The effect of using different analytic functions for $\Gamma(R)$ is, however, small and our analysis cannot establish uniquely the functional dependence of $\Gamma(R)$.

The principal parameters associated with $\Gamma(R)$, namely, R_x and F, can be determined to within $\pm 0.02a_0$ and ±10%, respectively, given the ionic potential. Except for $Cl^- + Ne$, the values of R_1 indicated in Table I represent upper bounds or, alternately viewed, they serve to limit the magnitude of $\Gamma(R)$ in the complex potential.

Finally, several comments should be made concerning the differences in the "semiclassical" method used in this investigation and the "classical" method of analysis employed in our earlier work.[1] First, the deflection functions $\Theta(b)$, as determined by each method, differ at most by 0.5% (they are, of course, exactly the same for $b > b_x$) in the large-angle (small-b) region. However, the results for the calculation of the survival probability $P_s(b)$ do depend upon the method employed, the difference increasing as b decreases. The semiclassical method always gives larger values for $P_s(b)$ than does the classical method. Quantitatively, rough agreement between differential cross-section calculations (i.e., semiclassical and classical) is achieved if one compares $\sigma_{classical}(\theta, F)$ to $\sigma_{semicl.}(\theta, 1.1F)$ when all other parameters in the calculation are identical.

ACKNOWLEDGMENTS

We would like to thank F. A. Kern for calibrating the capacitance manometer and B. T. Smith for his assistance in the experiments.

APPENDIX: THRESHOLD EFFECTS

Two processes are normally considered responsible for the production of free electrons in collisions of negative ions with atoms; (i) direct collisional detachment and (ii) associative detachment. Both processes are usually described as the result of the crossing of the ionic state with the corresponding neutral molecular state plus a free electron. Associative detachment, $A^- + B \rightarrow AB + e$, is possible when a bound state(s) exist for the molecule AB, whereas, only collisional detachment, $A^- + B \rightarrow A + B + e^-$, can occur if AB has no bound state(s).

With some exceptions, associative-detachment cross sections are usually large at thermal energies whereas direct-detachment processes have thresholds at relative collision energies which are normally greater than the electron affinity of A. Experiments which attempt to obtain thresholds from total-cross-section measurements for direct-collisional-detachment processes can be subject to large errors due in part to (a) thermal motion of the target gas, (b) spreads in primary-beam energy, and (c) the theoretical behavior of the cross sections near threshold.

The general problem of Doppler broadening in beam experiments has been considered in detail by Chantry.[9] To illustrate how serious these effects are in determining detachment thresholds from the experimental cross sections just presented, we will take a detailed look at the threshold region for $Cl^- + Ne$.

The measured and calculated total-detachment cross sections, in the neighborhood of threshold, are shown in Fig. 7. The calculated cross section has been convoluted with a Gaussian distribution (FWHM ~ 5 eV); the convoluted cross section is also shown in Fig. 7.

It should be noted that the calculated cross section has an extremely small slope from threshold to approximately 1 eV above threshold, then rises almost linearly at higher energies. If one were investigating a system whose true cross section had this general shape near threshold, and could eliminate all experimental broadening effects, it is very likely that the threshold inferred from the experiment would still be considerably higher than the true threshold. For cases where the true cross sections have essentially zero slope at threshold, broadening effects may actually reduce the error in determining the threshold. This can be seen in Fig. 7, where a linear extrapolation of the linear portion of the convoluted cross section gives a fair estimate of the threshold.

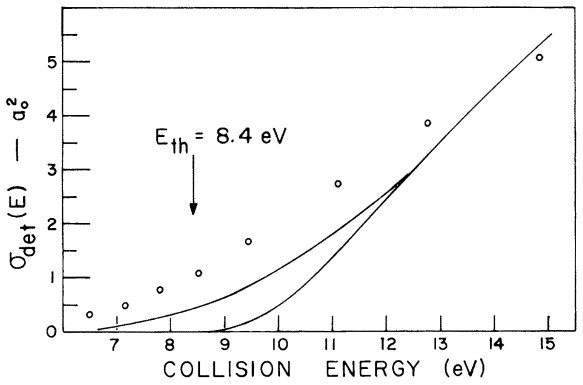

FIG. 7. Absolute total-detachment cross section near the threshold for $Cl^- + Ne$. The open circles are the experimental points and the solid lines are the calculated and convoluted cross sections. The parameters in Table I were used in the calculations.

It is obvious from Fig. 7 that our data does not fit the convoluted calculated cross section in the threshold region. This can be due to several reasons. First, $V(R_x)$ as retrieved from the experiments may be in error. However, all four experimental results show this same behavior, which indicates that some systematic effect may be responsible for the disagreement. It has been observed in this laboratory that negative-ion beams produced in a duoplasmatron source tend to have asymmetric energy distributions. Specifically, they exhibit high energy tails due to the preferential formation of negative ions near the cathode of the ion source. Such an asymmetric energy distribution of the primary ion beam could cause our extensive broadening of the true cross section when large positive slopes are involved, as is the case here.

[1]S. K. Lam, J. B. Delos, R. L. Champion, and L. D. Doverspike, Phys. Rev. A 9, 1828 (1974).
[2]A. J. H. Boerboom, H. Van Dop, and J. Los, Physica (Utr.) 46, 458 (1970).
[3]R. G. Gordon and Yung Sik Kim, J. Chem. Phys. 56, 3122 (1972).
[4]R. L. Champion, L. D. Doverspike, W. G. Rich, and S. M. Bobbio, Phys. Rev. A 2, 2327 (1970).
[5]J. C. Y. Chen, *Advances in Radiation Chemistry*, edited by M. Curtan and J. L. Magee (Wiley, New York, 1968), Vol. 1, p. 245 ff.
[6]J. Mizuno and J. C. Y. Chen, Phys. Rev. A 4, 1500 (1971).
[7]The values of the energy E and the angle θ refer to the c.m. coordinate system in this and following expressions and figures unless specifically stated otherwise.
[8]T. F. O'Malley, Phys. Rev. 155, 59 (1967).
[9]P. J. Chantry, J. Chem. Phys. 55, 2746 (1971).